

Mechanosensitive Gene Regulation by Myocardin-Related Transcription Factors is Required for Cardiomyocyte Integrity in Load-Induced Ventricular Hypertrophy

Running Title: *Trembley et al.; Transcriptional Control of Cardiomyocyte Integrity*

Michael A. Trembley, PhD^{1,2}; Pearl Quijada, PhD²; Esperanza Agullo-Pascual, PhD⁹;
Kevin M. Tylock, MS¹; Mert Colpan, PhD⁷; Ronald A. Dirkx, Jr., BS²; Jason R. Myers, MS⁵;
Deanne M. Mickelsen, BS²; Karen de Mesy Bentley, MS³; Eli Rothenberg, PhD¹⁰;
Christine S. Moravec, PhD⁸; Jeffrey D. Alexis, MD⁴; Carol C. Gregorio, PhD⁷;
Robert T. Dirksen, PhD¹; Mario Delmar, MD, PhD⁹; Eric M. Small, PhD^{1,2,6*}

¹Department of Pharmacology and Physiology, University of Rochester, Rochester, NY; ²Aab Cardiovascular Research Institute, Department of Medicine, University of Rochester, Rochester, NY; ³Department of Pathology, University of Rochester, Rochester, NY; ⁴Division of Cardiology, Department of Medicine, University of Rochester, Rochester, NY; ⁵Genomics Research Center, University of Rochester, Rochester, NY; ⁶Department of Biomedical Engineering, University of Rochester, Rochester, NY; ⁷Department of Cellular and Molecular Medicine, Sarver Molecular Cardiovascular Research Program, University of Arizona, Tucson, AZ; ⁸Department of Molecular Cardiology, Cleveland Clinic, Cleveland, OH; ⁹The Leon H Charney Division of Cardiology, Department of Medicine, New York University School of Medicine, New York, NY; ¹⁰Department of Biochemistry and Molecular Pharmacology, New York University School of Medicine, New York, NY

***Address for Correspondence:**

Eric M. Small, PhD
Aab Cardiovascular Research Institute
University of Rochester School of Medicine and Dentistry
601 Elmwood Avenue, Box CVRI
Rochester, NY 14642
Tel: (585)276-7706
Fax: (585) 276-9839
Email: Eric_Small@URMC.rochester.edu

Abstract

Background—Hypertrophic cardiomyocyte (CM) growth and dysfunction accompanies various forms of heart disease. The mechanisms responsible for transcriptional changes that impact cardiac physiology and the transition to heart failure (HF) are not well understood. The intercalated disc (ID) is a specialized intercellular junction coupling CM electrical activity and force transmission, and is gaining attention as a mechanosensitive signaling hub and hotspot for causative mutations in cardiomyopathy.

Methods—Transmission electron microscopy, confocal microscopy, and single-molecule localization microscopy (SMLM) were used to examine changes in ID structure and protein localization in the murine and human heart. We conducted detailed cardiac functional assessment and transcriptional profiling of mice lacking myocardin-related transcription factor-A (MRTF-A) and –B specifically in adult CMs to evaluate the role of mechanosensitive regulation of gene expression in load-induced ventricular remodeling.

Results—We found that MRTFs localize to IDs in the healthy human heart and accumulate in the nucleus in heart failure (HF). Although mice lacking MRTFs in adult CMs display normal cardiac physiology at baseline, pressure overload leads to rapid HF characterized by sarcomere disarray, ID disintegration, chamber dilation and wall thinning, cardiac functional decline, and partially penetrant acute lethality. Transcriptional profiling reveals a program of actin cytoskeleton and CM adhesion genes driven by MRTFs during pressure overload. Indeed, conspicuous remodeling of gap junctions at IDs identified by SMLM may partially stem from a reduction in *Mapre1* expression, which we show is a direct mechanosensitive MRTF target.

Conclusions—Taken together, our study describes a novel paradigm in which MRTFs control an acute mechanosensitive signaling circuit that coordinates crosstalk between the actin and microtubule cytoskeleton and maintains ID integrity and CM homeostasis in heart disease.

Key Words: MRTF-A; MRTF-B; Mkl1; Mkl2; cardiac hypertrophy; cardiac remodeling; intercalated disc

Clinical Perspective

What is new?

- Myocardin-related transcription factors (MRTFs) associate with desmosome proteins of the intercalated disc (ID) in murine and human hearts.
- Genetic deletion of MRTFs in cardiomyocytes leads to rapid onset of dilated cardiomyopathy in response to pressure overload-induced hypertrophy.
- MRTFs are required for the maintenance of sarcomere and ID integrity under pathological stress.
- Proper gap junction trafficking requires MRTF-dependent transcription of the mechanosensitive gene, *Mapre1*.

What are the clinical implications?

- Here, we show that adaptation to pressure overload requires stress-responsive signaling is mediated by MRTFs.
- These findings provide a unique link between the ID and mechanosensitive transcriptional regulation.
- MRTFs redistribute from the ID in human heart failure, which may represent a novel signaling complex present in cardiomyopathies characterized by desmosome dysfunction.



Introduction

Heart disease of various etiologies is associated with increased cardiac mass due to hypertrophic growth and remodeling of cardiomyocytes (CMs) ¹. This process was initially proposed to increase cardiac output in response to excessive afterload and was termed compensatory hypertrophy. However, multiple preclinical studies have since found that blocking hypertrophic cardiac growth improves cardiac function ². Indeed, changes in CM structure and physiology ultimately impair contractility and drive the progression of heart failure (HF), the leading cause of death in the United States ³. Thus, it is currently not clear whether physiological adaptations to pathological signals provide a cardiac benefit.

CMs respond to pathological stimuli such as pressure or volume overload, biomechanical stress, and inherited mutations by inducing discrete gene expression programs that increase the synthesis of structural proteins ^{1,4}. Serum response factor (SRF) is a highly conserved and ubiquitously expressed transcription factor that directly binds to specific nucleotide sequences called CArG boxes (CC(A/T)₆GG) ⁵, that are found upstream of many genes encoding actin cytoskeleton, extracellular matrix (ECM), and cardiac muscle structural proteins ⁶. The ability of SRF to control gene expression largely depends on the availability of transcriptional co-factors, such as myocardin-related transcription factors (MRTF)-A (MKL1, MAL, or BSAC) and MRTF-B (MKL2) ⁷. G-actin sequesters MRTFs in the cytoplasm by concealing their nuclear localization sequence ^{8,9}. Actin polymerization mediated by serum stimulation, mechanical tension, and/or Rho-kinase (ROCK) activation allows MRTFs to accumulate in the nucleus where they stimulate SRF-dependent transcription ⁹. Deletion of either SRF or MRTFs in the embryonic heart is incompatible with life ¹⁰⁻¹². We and others have shown that MRTF-A promotes survival and cardioprotective signals via the miR-486/PI3K/AKT pathway ¹³ or

through the upregulation of the matricellular protein, cysteine-rich angiogenic inducer 61 (*Cyr61* or *Ccn1*) in ischemia reperfusion¹⁴. However, MRTF-A also mediates hypertrophic signaling in adult CMs and drives the expression of brain natriuretic peptide (*Nppb*, BNP) in response to mechanical and neurohumoral stimuli¹⁵. Although SRF and MRTFs have emerged as critical mediators of cellular plasticity by linking changes in the actin cytoskeleton with mechanosensitive gene expression programs¹⁶, their function in adult CM physiology remains elusive.

Transmission of mechanical force between adjacent CMs occurs at specialized intercellular junctions called intercalated discs (IDs)¹⁷. The ID is composed of desmosomes, adherens junctions, and gap junctions, creating an environment in which mechanical tension and electrical communication are directly coupled^{18,19}. IDs have been traditionally viewed as cell-cell adhesion and communication centers; however, emerging evidence has redefined this view, suggesting that IDs are a hub for signaling pathways such as Rho-ROCK, Hippo and Wnt²⁰⁻²³. Indeed, myocardium-enriched zona occludens-1-associated protein (myozap), which is localized to IDs, regulates mitogen-activated protein kinase (MAPK) and MRTF/SRF activity, suggesting a potential link between the ID and mechanosensitive transcriptional regulation²⁴.

Here, we find that MRTFs are enriched at IDs in the healthy murine and human heart, and accumulate in the nucleus during HF. While genetic deletion of MRTF-A and MRTF-B in CMs (called MRTF^{dKO}) does not alter normal adult cardiac physiology, MRTF^{dKO} mice are exquisitely sensitive to pressure overload-induced cardiac remodeling. MRTF^{dKO} mice rapidly develop dilated cardiomyopathy following transverse aortic constriction (TAC), characterized by eccentric hypertrophy, sarcomere disarray and ID disintegration, and exhibit partially penetrant lethality. MRTFs drive a program of gene expression in CM during hypertrophic remodeling that

includes actin cytoskeleton, adhesion, and gap junction trafficking genes. Among these genes, our study identifies *Mapre1*, a novel mechanosensitive MRTF target that is critical for normal Cx43 localization at the ID. Using a combination of advanced methods including single molecule localization microscopy (SMLM), mislocalization of Cx43 was observed in MRTF-null CMs. Taken together, these data reveal a transcriptional adaptation to pressure overload driven by MRTFs that fortifies CM integrity. The association of MRTFs to IDs may represent a novel paradigm by which MRTFs coordinate mechanosensitive signaling critical for maintaining CM homeostasis in heart disease.

Methods



These data and study materials will be made available to other researchers for purposes of reproducing the results or replicating the procedure. RNA-sequencing data has been submitted to the Gene Expression Omnibus (GEO) as GSE102792.

Human Samples

Human tissues were obtained from the Kaufman Center for Heart Failure Tissue Bank at Cleveland Clinic or the University of Rochester with Institutional Review Board (IRB) approval and patient consent.

Mice

All experiments using animals were approved by the University Committee on Animal Resources at the University of Rochester. *Mrtfa*^{-/-}, *Mrtfb*^{flox} and α -MHC^{MerCreMer} mice were previously described and maintained on a C57BL/6J background²⁶⁻²⁸. Inducible Cre-mediated recombination, TAC procedure, and echocardiography are described in Supplemental Methods.

Plasmids and cloning

Plasmids expressing FLAG-plakophilin 2 and myc-plakoglobin were obtained from Addgene (stock numbers 32230 and 32228); FLAG-MRTF-A and HA-MRTF-A were previously described⁷. *Mapre1* promoter cloning and mutagenesis are described in Supplemental Methods, and primers are listed in Supplemental Table 1.

Cell culture and transfection

COS7 and NIH3T3 cells were cultured as recommended (ATCC) and transfected using Lipofectamine 2000 (ThermoFisher) or *TransIT*-X2 (Mirus), respectively. Luciferase activity was detected using a luciferase assay kit (Promega) on a FLUOstar Optima plate reader (BMG Labtech, Cary, NC). Details are provided in Supplemental Methods.



Neonatal mouse ventricular myocytes

NVMs were isolated from P0 hearts using a gentleMACS Octo Dissociator (Miltenyi, Auburn, CA) and differential plating as described in Supplemental Methods. For overexpression studies, wildtype NVMs were transduced with a beta-galactosidase or MRTF-A expressing adenovirus (1×10^5 pfu/ml) and cultured for 48 hrs. For deletion studies, *Mrtfa*^{-/-}; *Mrtfb*^{fl^{ox}/fl^{ox}} NVMs were transduced with an adenovirus expressing beta-galactosidase or Cre recombinase (Ad/Cre; 1×10^6 pfu/ml) and cultured for 72 hrs. For stretch experiments, 1×10^6 NVMs were seeded onto $30 \times 30 \text{ mm}^2$ silicon chambers (Strex, San Diego, CA) pre-coated with $50 \mu\text{g/ml}$ collagen I (BD Biosciences). Cells were subjected to 20% uniaxial stretch at 1 Hz for 4hrs using a stretch apparatus (Scholar Tec, Osaka, Japan; Model NS-500).

Adult cardiomyocytes

Adult CMs and non-CMs were isolated by Langendorff perfusion as described in Supplemental Methods.

Co-immunoprecipitation

Co-immunoprecipitation was performed on COS7 lysates as described in Supplemental methods.

Antibodies used for co-IP and Western blot analysis are found in Supplemental Table 2.

RNA isolation and analysis

Total RNA was isolated from cells or tissue samples using Trizol reagent (Ambion). cDNA was generated from 1 µg of RNA using the iScript Reverse Transcriptase Kit (BioRad) and qRT-PCR was performed with SYBR-Green mastermix (BioRad) on a CFX Connect (BioRad). qRT-PCR primer sequences are listed in Supplemental Table 1.

RNA-sequencing and differential gene expression analysis

Total RNA was isolated using Trizol reagent (Ambion) and genomic DNA was removed with the TURBO DNase I kit (Ambion). RNA concentration and quality was assessed with the Agilent Bioanalyzer (Agilent, Santa Clara, CA). Library construction was prepared using the TruSeq RNA sample Preparation Kit (Illumina) and sequenced using an Illumina HiSeq2500 (Illumina, Santa Clara, CA) with a read depth of 20-25 million reads at 1x100bp. Details on analysis of RNA-sequencing data are described in the Supplementary Methods.

Chromatin immunoprecipitation

ChIP was performed on CM chromatin using the EZ ChIP Kit (Millipore) with slight modifications as described in Supplemental Methods. Antibodies and qRT-PCR parameters are listed in Supplemental Tables 1 and 2.

Histology, immunohistochemistry, and immunocytochemistry

Cardiac morphology was assessed with hematoxylin & eosin staining. Tissue fibrosis was assessed with Picrosirius Red stain (Abcam), visualized with polarized light on an Olympus BX51 microscope, and quantified with Image J (NIH). Immunohistochemistry and

immunocytochemistry details are listed in Supplemental Methods. All fluorescent images were acquired using an inverted scanning confocal microscope (Olympus 1X81). Myocyte length and width measurements were performed using FluoView software (Olympus). Antibodies and immunostaining conditions are listed and Supplemental Table 2.

Transmission electron microscopy

Hearts slices were isolated from 14-week old male mice and immediately fixed in 2.5% glutaraldehyde buffered with 0.1 M sodium cacodylate. Samples were post-fixed in 1% osmium tetroxide, dehydrated in ethanol, transitioned into propylene oxide, and then transferred into Epon/Araldite resin. Tissues were embedded into molds containing fresh resin and polymerized for 2 days at 65°C. 70nm sections were placed onto carbon-coated Formvar slot grids and stained with aqueous uranyl acetate and lead citrate. The grids were examined using a Gatan 11 megapixel Erlansheng digital camera and Digital micrograph software.

Single Molecule Localization Microscopy

Isolated CM were plated on laminin coated coverslips and fixed with 4% paraformaldehyde in PBS for 10 min (Cx43 labeling) or cold methanol for 3 min (EB1 labeling). Cells were permeabilized with 0.1% Triton x-100 for 10 min, blocked in PBS containing 2% bovine serum albumin, 2% glycine and 0.2% gelatin for 30 min, and incubated with primary antibodies for 1 hour. Samples were imaged in a custom-built microscopy set up⁴⁹. Total internal reflection fluorescence (TIRF) or highly inclined illumination (HILO) modes with solid-state lasers 556 and 640nm were used to excite the samples and improve the signal-to-noise ratio. Imaging conditions were achieved by addition of 200 mM mercaptoethylamine and an oxygen scavenging system (0.04 mg/ml glucose oxidase, 0.8 µg/ml catalase and 10% (wt/wt) glucose). 2,000 frame movies of each channel were acquired sequentially and aligned using an IDL (Exelis Visual

Information Solutions) custom mapping routine⁴⁹. See the Supplementary Methods for staining conditions and analysis of SMLM images.

Statistical Analysis

All statistical analyses were performed using Prism software (GraphPad) and data represented as mean +/- SEM. Two groups were compared using student T-tests. Multiple groups were compared using one or two-way ANOVA test and Tukey's post-hoc tests and repeated measures as indicated in figure legends. Kaplan-Meier method was used to estimate survival, and survival curves were compared using the Mantel-Cox test. Significance is defined as $P < 0.05$.

Results



MRTFs are enriched at intercalated discs and redistribute in human HF

In order to interrogate the activity of MRTFs in a highly complex actin network such as the CM we initially evaluated their localization by immunohistochemistry on sections of normal neonatal and adult mouse hearts (Figure 1). MRTFs are broadly distributed at postnatal (P) day 7.

Coincident with ID maturation at P21, these foci co-localize with the desmosome proteins, plakophilin 2 (PKP2), plakoglobin, and desmoplakin (Figure 1 and Supplemental Figures 1A – D)²⁵. Surprisingly, we often observe MRTFs in the cytoplasm and nucleus following pressure overload induced ventricular remodeling (TAC), although the majority of MRTFs remain at the ID (Supplemental Figure 2).

We next performed immunohistochemistry on sections obtained from healthy or failing human hearts to evaluate the evolutionary conservation of MRTF localization and relevance to human disease (Supplemental Table 3). MRTFs are again highly enriched at IDs of the healthy human heart, becoming more diffusely distributed throughout the CM in fibrotic regions of

failing hearts, and occasionally accumulating in the nucleus (Figure 2A-B and Supplemental Figure 3A). MRTFs also appear to accumulate in the cytoplasm in HF as assessed by Western analysis of left ventricle protein lysates, although we observe considerable variability in mRNA and protein levels, and enrichment in the nucleus was not evident (Supplemental Figure 3B-H).

Co-immunoprecipitation revealed that MRTF-A interacts with PKP2 and actin (Figure 2C). PKP2 reduces the association between MRTF-A and actin, suggesting the interaction between MRTF and PKP2 or actin is mutually exclusive (Figure 2C-D). These data indicate MRTFs may be anchored to regions of CM force transmission and suggest changes in mechanical tension and actin dynamics in disease may lead to altered affinity of MRTFs for the ID.



MRTFs are dispensable in CM for adult cardiac homeostasis

MRTFs are essential in CMs for normal heart development¹¹, but their role in the adult heart is unclear. Therefore, we utilized the CM-specific and tamoxifen-inducible α -MHC^{MerCreMer} mouse line²⁶ to delete *Mrtfb*²⁷ in adult mice harboring a global *Mrtfa* deletion²⁸. To induce *Mrtfb* deletion, eight-week old mice were administered tamoxifen (30mg/kg) for three consecutive days (MRTF^{dKO}, Supplemental Figure 4A); controls were tamoxifen-administered α -MHC^{MerCreMer} mice on an otherwise wildtype background. Recombination was observed in ~70% of CM, leading to ~ 50% reduction of *Mrtfb* mRNA levels in CM and reduction of MRTF protein levels and SRF target gene expression (Supplemental Figure 4B-E). Surprisingly, serial echocardiographic analysis revealed normal cardiac physiology up to at least one year post-tamoxifen injection (Supplemental Table 4). We conclude that after cardiac maturation MRTFs are no longer required for maintenance of baseline cardiac homeostasis.

MRTF deletion results in functional decline with pressure overload

Given the role of MRTFs in mechanosensitive signaling^{29,30} and their redistribution in human HF and following TAC surgery, we asked whether MRTFs contribute to pressure overload-induced ventricular remodeling (Figure 3A). In stark contrast to control mice, MRTF^{dKO} mice exhibited 50% lethality within 4 days of TAC surgery; only ~34% of MRTF^{dKO} mice survived to 28 days post-TAC (Figure 3B). We speculated that premature lethality might arise from perturbed electrical activity that manifests in arrhythmias. Mice were implanted with radiotelemeters at the time of TAC surgery and we recorded for continuous, conscious electrocardiograms (ECGs) for 7 days. MRTF^{dKO} mice that died prematurely displayed a gradual slowing of their heart rate, a marked decline in body temperature, and became severely lethargic but did not leave sinus rhythm (data not shown). Calculated standard ECG parameters for all MRTF^{dKO} mice maintaining normal body temperature after TAC were not significantly different from controls (Supplemental Figure 5A-E). It should be noted that, while MRTF^{dKO} mice did not exhibit signs of arrhythmia, we were unable to confidently calculate the QT-interval because of drastic changes to T-wave morphology.

Serial echocardiography revealed rapid and robust decline in cardiac performance in MRTF^{dKO} mice only when subject to TAC. Of the MRTF^{dKO} mice surviving to 7-days post-TAC, ejection fraction (EF) and fractional shortening (FS) reduced by 66% and 78%, respectively, continuing to decline until the experimental endpoint (Figure 3C-D). Although control and MRTF^{dKO} animals exhibit an equivalent increase in heart mass following TAC (Figure 3E), control mice develop concentric hypertrophy whereas MRTF^{dKO} hearts appear dilated (Figure 3F). Analysis of the fetal cardiac gene program was performed to gauge HF severity, revealing exaggerated myosin heavy chain (MHC) isotype switching (*Myh6* versus *Myh7*) after TAC in

MRTF^{dKO} mice compared to controls (Figures 3G-H). However, *Nppb* expression did not show an exaggerated increase after TAC, and *Acta1* expression is attenuated in the MRTF^{dKO} hearts even after TAC, consistent with reports that *Nppb* and *Acta1* are direct target genes of SRF^{15, 31} (Figure 3I-J). Elevated levels of periostin (*Postn*) expression in MRTF^{dKO} hearts compared to controls following TAC indicated exaggerated myofibroblast activation (Supplemental Figure 6A)³². However, we did not observe significant differences in the expression of ECM genes (Supplemental Figures 6B-D) or excessive fibrosis in MRTF^{dKO} hearts (Supplemental Figures 6E-I). Taken together, the increased mortality of MRTF^{dKO} mice following TAC was likely not the result of fatal arrhythmias and instead suggests a susceptibility to dilated cardiomyopathy.

MRTF deletion results in cardiac dilatation and loss of CM structural integrity



MRTF^{dKO} hearts display a pronounced increase in left ventricular volumes (LVESV and LVEDV) and internal diameters (LVIDs and LVIDd) following TAC (Figures 4A-D).

Furthermore, MRTF^{dKO} hearts exhibit left ventricular wall thinning even in the context of equivalent hypertrophic growth (Figure 4E-H). To determine if differences in CM shape might account for the apparent dilatation, immunohistochemistry was performed to label CM lateral borders with wheat germ agglutinin (WGA) and Cx43 to label IDs (Figure 4I). As expected, TAC leads to reduced length-to-width ratio in control hearts, characteristic of concentric hypertrophy. In contrast, CM length-to-width ratio significantly increased in MRTF^{dKO} animals following TAC surgery, indicative of dilated or eccentric hypertrophy (Figure 4J-L). Of note, Cx43 was partially mislocalized in MRTF^{dKO} hearts compared to controls, which may further indicate a propensity for HF³³.

Next, we performed transmission electron microscopy (TEM) to assess ultrastructural changes in CM following TAC. We observed close apposition of IDs at adjacent CMs in both

control and MRTF^{dKO} mice subjected to sham surgery (Figure 5A-a, 5A'-a', Supplemental Figure 7A). While MRTF deficiency did not impair ID integrity at baseline, CM interdigitation seemed more apparent (Figure 5A-b, 5A'-b', Supplemental Figure 7A). As expected, ID interdigitation was increased following TAC in control animals without obvious defects to the myofibrillar organization (Figure 5A-c, 5A'-c', Supplemental Figure 7A). In contrast, ID morphology was profoundly disrupted in MRTF^{dKO} hearts following TAC (Figure 5A-d, 5A'-d', Supplemental Figure 7A). Specifically, IDs were highly irregular and distorted, displaying lacunae filled with vacuole-like structures near the plicate regions (asterisks in Figure 5A-d, 5A'-d'). Intercellular junctions remained in close apposition whereas myofibril organization and attachment to the ID was severely compromised. Abnormal ID morphology may reflect alterations in tensile strength at the sarcomere, which receives and generates mechanical force. At baseline, hearts from control and MRTF^{dKO} mice displayed organized sarcomeres with clear demarcations between A-bands, I-bands and electron dense Z-discs (Figure 5B, Supplemental Figure 7B). While TAC did not alter the sarcomere in control mice, pressure overload resulted in extreme sarcomere disarray in MRTF^{dKO} mice, characterized by diffuse contractile bands and shorter distances between Z-discs (Figure 5B-C). Notably, the M-line is nearly undetectable in MRTF^{dKO} mice after TAC. Sarcomere disarray is associated with alterations in the localization of myosin thick filaments, myomesin at the M line, as well as Z and I band regions of titin, as demonstrated by immunofluorescence deconvolution imaging of heart sections obtained from an MRTF^{dKO} mouse captured at the time of death (late stage) (Supplemental Figures 8 and 9, respectively). It appears that myosin and titin disruption is not a primary phenotype, since we did not observe disorganization of these filaments in early stage disease that is already associated

with considerable dilation. Interestingly, F-actin and myosin binding protein-C in the A band (which interacts with filamentous actin) was not affected, even at late stage of disease.

To evaluate the nano-scale organization of ID proteins and confirm disruption in Cx43 localization, we performed dual-color single-molecule localization microscopy (SMLM)³⁴. Although the area of IDs and size of Cx43 clusters were unchanged in MRTF⁻ depleted CM relative to controls (Supplemental Figure 10A-B), MRTF^{dKO} CM exhibit a significant reduction in Cx43 cluster density within 500 nm of the ID plicate region (Figure 6A - B), and an increase in distance to the nearest Cx43 cluster (Figure 6C). These findings suggest a possible defect in Cx43 trafficking to the ID upon MRTF deletion. EB1 (*Mapre1*) is the best characterized microtubule-based plus-end trafficking protein implicated in anterograde trafficking of cardiac gap junctions³⁵. SMLM revealed normal density of EB1 clusters within 500 nm of the ID in MRTF^{dKO} CM (Supplemental Figures 10C-D). However, the proximity of EB1 clusters to the ID in MRTF deficient CMs is altered, with more clusters found distal to N-cadherin (Figures 6D – E). This trend of reduced association of EB1 with the ID could impair delivery of Cx43 and lead to diffuse localization. Indeed, acute deletion of MRTFs in neonatal ventricular myocytes (NVMs), did not impact gap junction mRNA levels, but altered Cx43 trafficking to the plasma membrane (Supplemental Figures 10E – H). Although a modest delay in fluorescence recovery after photobleaching (FRAP) was observed in MRTF-deficient NVMs, alterations in the kinetics of CM communication did not reach statistical significance (Supplemental Figures 10I – K). These data indicate MRTFs are critical for maintenance of sarcomere structure and ID integrity during ventricular pressure overload.

MRTF-dependent transcriptional adaptation in load induced ventricle remodeling

To investigate the acute transcriptional changes underlying the loss of CM structural integrity and premature lethality in MRTF^{dKO} mice, we conducted RNA-sequencing (RNA-seq) of CMs isolated from control and MRTF^{dKO} mice at 7 days post-TAC (Figure 7A, Supplemental Figures 11A – B). *Myh6* and *Tcf21* expression confirmed purity of the CM and fibroblast populations, respectively (Supplemental Figures 11C – D), and alterations in select stress-responsive genes confirmed pressure overload induced remodeling (Supplemental Figures 11E – P). Principle component analysis revealed clustering of biological replicates while the transcriptomes of each experimental group diverged, suggesting transcriptional changes may contribute to phenotypic differences (Supplemental Figure 11Q). Consistent with the finding that baseline cardiac function is unaltered upon MRTF deletion, we observed the least variation in gene expression (73 genes) between sham operated MRTF^{dKO} and control mice (Figure 7A). In contrast, 347 differentially expressed genes (DEGs; 117 down- and 230 up-regulated) were identified between control and MRTF^{dKO} mice subjected to TAC (Figure 7A).

Ingenuity Pathway Analysis (IPA) was used to identify dysregulated signaling pathways and transcriptional regulators in CMs from MRTF^{dKO} mice following TAC (Figure 7B – C). Importantly, SRF was predicted to be the most likely transcriptional regulator of DEGs (Figure 7B). DEGs defined an enrichment in pathways related to tight junctions, integrins, and adherens junctions (Figure 7C). Integrin-linked kinase (ILK) and actin cytoskeletal signaling were predicted to be significantly inhibited. Conversely, Rho GDP-dissociation inhibitor (GDI) signaling, a negative regulator of Rho GTPases, was predicted to be activated in MRTF^{dKO} CM. Thus, deletion of MRTFs in CM subjected to pressure overload impacts various pathways involved in cell-cell adhesion and actin dynamics.

We next performed gene ontology (GO) analyses to define biological processes associated with a transcriptional response to pressure overload that are dysregulated by MRTF deletion. The biological processes that were most disrupted included GO terms such as muscle contractility and muscle filament sliding (Figure 7D). Consistent with ID disintegration observed by TEM, transcripts that encode components of the ID and adherens junctions were the most significantly altered in CM of MRTF^{dKO} mice subjected to pressure overload (Figure 7E). Indeed, the expression of various junctional proteins is altered 2 weeks following tamoxifen-inducible MRTF deletion (Supplemental Figure 11R).

Since MRTF^{dKO} mice quickly succumb to heart failure following TAC, we hypothesized that MRTF^{dKO} mice lack a transcriptional program required to respond to cardiac stress. Therefore, we performed hierarchical clustering to identify genes that are dependent upon MRTF (Clusters 5-8; Figure 7F). These clusters are enriched in genes that encode actin and effectors of the actin cytoskeleton, some of which were validated by qRT-PCR (Figure 7F, Supplemental Figures 11S-V). Given the role of MRTFs in mechanosensitive transcription, we assessed whether mechanical tension *in vitro* promotes the expression MRTF-dependent gene targets identified by our RNA-seq. Indeed, stretch-induced expression of actin genes and *Nppb*¹⁵ in NVMs require MRTFs (Figures 7G – J). Our study indicates that MRTFs are required for stress-dependent induction of actin and adhesion gene programs in response to pressure overload.

MRTFs regulate gap junction trafficking

Gap junction trafficking to the ID requires the coordinated action of the microtubule-based molecular motors, scaffolding proteins, and the actin cytoskeleton³⁵⁻³⁷. Thus, we evaluated whether ultrastructural defects in IDs of MRTF^{dKO} hearts coupled with transcriptional deficiencies in actin-based gene programs may be linked to alterations in microtubule-based

trafficking programs. We found that *Mapre1*, *Dctn1*, and *Kif5b* transcripts were all reduced in CMs from MRTF^{dKO} mice, while Cx43 (*Gjal*) mRNA levels were unchanged (Figure 8A). Furthermore, forced overexpression of MRTF-A in NVMs was sufficient to induce the expression of *Mapre1*, *Kif5b*, *Dctn1*, and the MRTF target gene, *Acta2* (Figure 8B). Consistent with mechanosensitive regulation of MRTF-dependent actin genes, stretch also induced the expression of *Mapre1* in control NVMs, but not in MRTF^{dKO} NVMs (Figure 8C). Upon closer inspection of the *Mapre1* promoter, we identified an evolutionarily conserved region containing a CArG box located between 24 and 33 nucleotides upstream of the transcription start site (Figure 8D), which was cloned into a luciferase reporter vector (Figure 8D, region denoted by red line). Forced expression of MRTF-A in NIH 3T3 cells induced the activity of a wildtype *Mapre1* reporter, but not a *Mapre1* reporter containing a CArG box mutation (Figure 8E). Furthermore, chromatin immunoprecipitation on whole heart lysates revealed SRF occupancy at both the *Mapre1* promoter and a control promoter (*Acta2*) (Figure 8F). Taken together, these data reveal a novel and unanticipated role for MRTFs in gap junction trafficking, potentially via stress-dependent regulation of the actin cytoskeleton and microtubule associated trafficking proteins. These results may also indicate a more general role for MRTFs in stabilizing the sarcomere and ID in response to ventricular pressure overload.

Discussion

In this study, we demonstrate that MRTF-A and -B are required for maintenance of CM integrity during load-induced ventricular hypertrophy. Mice lacking MRTFs in adult CM undergo rapid dilatation and HF characterized by sarcomere disarray and ID disintegration. RNA-sequencing revealed numerous genes related to the sarcomere, ID, and muscle contraction that failed to be

induced by pressure overload in MRTF-null mice. We found that the Cx43 trafficking protein, *Mapre1*, is a direct mechanosensitive target of MRTFs, linking stress dependent alterations in the actin cytoskeleton to microtubule-based trafficking to the ID. Taken together, conspicuous localization of MRTFs to the ID creates a novel paradigm of mechanosensitive transcriptional adaptation that supports ID integrity and CM contractility in pressure overload induced cardiac remodeling.

Context-dependent roles for the myocardin family of transcription factors

Our bioinformatics analysis revealed SRF as the most likely transcriptional activator of genes that are dysregulated in MRTF^{dKO} CMs, consistent with genome-wide chromatin occupancy studies linking MRTFs to promoters and enhancers containing SRF-responsive CA_TG boxes³⁸. However, while *Srf* deletion in adult CMs leads to rapid dysfunction^{31, 39}, we find that MRTF^{dKO} mice display normal cardiac physiology for up to a year after tamoxifen administration. Our finding also contrasts the rapid postnatal death observed upon deletion of MRTFs in fetal CMs¹¹. Sequestration of MRTFs at the ID in the healthy adult heart may provide a simple explanation for these apparent discrepancies, particularly if MRTFs are poised at the ID as a sensor of mechanical tension. MRTFs appear more diffuse within the embryonic and early postnatal CMs, only accumulating with other desmosome proteins upon ID maturation at ~ P21. It is possible that MRTFs are active contributors to CM maturation in the early postnatal period, becoming dormant following accumulation at the ID of the healthy adult heart. Further study is required to evaluate the potential that MRTF-A and -B have distinct transcriptional roles, or even whether MRTFs may constitute a structural component of the ID. Myocardin, which is constitutively active and necessary and sufficient to induce SRF-dependent cardiac gene expression, apparently compensates for MRTF loss only in the healthy adult heart^{40, 41}. Thus, the heart seems

particularly sensitive to perturbations of SRF/MRTF gene expression during postnatal CM maturation and pressure overload-induced ventricular remodeling, indicating a unique requirement for SRF/MRTF dependent gene programs that support actin based sarcomere integrity and adhesions to the ID.

ID integrity requires MRTF-dependent regulation of the actin and microtubule cytoskeleton

The ID is composed of a complex of adhesion molecules, ion channels, and gap junctions. Recent advances in nano-scale imaging has revealed functional interdependence between individual components of the ID. For example, Cx43 disruption alters targeting of NaV1.5 to the ID and NaV1.5 contributes to N-cadherin dependent CM adhesions^{34, 42}. Thus, regulation of Cx43 trafficking by MRTFs identified in this study may have a greater impact on ID structure and function than currently realized. Connexins are dynamically shuttled to and from the ID via distinct anterograde and retrograde trafficking machineries. Microtubule plus-end-tracking proteins, such as EB1 (*Mapre1*), are critical for efficient delivery and transfer of Cx43 to the ID³⁵. In addition to the microtubule cytoskeleton, Cx43 associates with β -actin and requires dynamic actin treadmilling en route to the ID³⁷. In this study, we suggest a mechanistic link in which MRTF-dependent transcription of *Mapre1* facilitates microtubule-based trafficking of ID cargo.

An ID-based mechanism controlling MRTF activity

A recent study revealed that the magnitude of mechanical tension governs the likelihood of developing concentric or dilated cardiomyopathy⁴³, suggesting that mechanosensitive regulation of gene expression by MRTFs may represent a feedback mechanism increasing CM tension and delaying the transition to dilated remodeling. We observe nuclear accumulation of MRTFs in the

myocardium of human heart failure biopsies; however, the mechanisms driving MRTF from the ID to the nucleus in heart disease are not apparent. MRTF-mediated transcription in mesenchymal cells is induced by loss of cell contacts, excessive mechanical tension, and RhoA-dependent signaling, primarily via modulation of actin dynamics^{9,44}. Since CM-restricted inactivation of RhoA also leads to dilated remodeling upon pressure overload⁴⁵, it is possible a similar regulatory mechanism exists in MRTF^{dKO} CMs. Indeed, we find that interactions between MRTFs and PKP2 or actin are mutually exclusive, suggesting that alterations in actin dynamics in disease may impact the affinity of MRTF for the desmosome. However, it is not evident how this would lead to accumulation of MRTF in the nucleus.

Mutations to several genes encoding desmosome proteins are correlated with the pathogenesis of arrhythmogenic right ventricular cardiomyopathy (ARVC), characterized by strain-dependent disintegration of the ID, fibro-fatty tissue deposition, arrhythmias, and sudden death⁴⁶. However, the mechanisms linking structural defects at the ID to the clinical manifestations of ARVC remain unclear. Evidence suggests that altered scaffolding of signaling molecules at the ID may be a substrate for dysregulated signaling pathways²⁰. Of note actin-binding Rho-activating protein (*Abra* or STARS), which modulates stress-responsive signaling of MRTF translocation in cultured CM⁴⁷, is among the most downregulated genes in ARVC patients⁴⁸. These findings, combined with our observations, hint at the possible involvement of MRTF signaling in ARVC; however, further investigation is warranted. We propose that MRTFs are necessary for mechanosensitive transcriptional adaptation to cardiac stress that maintains CM integrity by fortifying the adhesion between the sarcomere and ID.

Acknowledgments

We thank David Auerbach and Scott Cameron for helpful suggestions and advice with electrophysiology and FRAP experiments. Guido Posern kindly provided the MRTF antibody.

Sources of Funding

This work was supported by grants from the NIH/NHLBI, including R01HL136179 to EMS and MD; R01HL120919 and R01HL133761 to EMS; R01GM57691 and R01HL134328 to MD; R01HL123078 to CCG; T32HL066988 and T32GM068411 to MAT; T90DE21985 and U54NS048843 to KMT; T32HL066988 and F32HL134206 to PJQ; the American Heart Association (16PRE3049000 to MAT); the Howard Hughes Medical Institute Med-Into-Grad program (HHMI 56006775 to MAT and KMT); and an Aab Cardiovascular Research Institute Pilot Study Award to EMS and JDA.

Disclosures

None

References

1. Hill JA, Olson EN. Cardiac plasticity. *N Engl J Med*. 2008;358:1370-1380.
2. Hill JA, Karimi M, Kutschke W, Davisson RL, Zimmerman K, Wang Z, Kerber RE, Weiss RM. Cardiac hypertrophy is not a required compensatory response to short-term pressure overload. *Circulation*. 2000;101:2863-2869.
3. Writing Group M, Mozaffarian D, Benjamin EJ, Go AS, Arnett DK, Blaha MJ, Cushman M, Das SR, de Ferranti S, Despres JP, Fullerton HJ, Howard VJ, Huffman MD, Isasi CR, Jimenez MC, Judd SE, Kissela BM, Lichtman JH, Lisabeth LD, Liu S, Mackey RH, Magid DJ, McGuire DK, Mohler ER, 3rd, Moy CS, Muntner P, Mussolino ME, Nasir K, Neumar RW, Nichol G, Palaniappan L, Pandey DK, Reeves MJ, Rodriguez CJ, Rosamond W, Sorlie PD, Stein J, Towfighi A, Turan TN, Virani SS, Woo D, Yeh RW, Turner MB, American Heart Association Statistics C, Stroke Statistics S. Executive

- summary: Heart disease and stroke statistics--2016 update: A report from the american heart association. *Circulation*. 2016;133:447-454.
4. Morita H, Seidman J, Seidman CE. Genetic causes of human heart failure. *J Clin Invest*. 2005;115:518-526.
 5. Sun Q, Chen G, Streb JW, Long X, Yang Y, Stoeckert CJ, Jr., Miano JM. Defining the mammalian cargoome. *Genome Res*. 2006;16:197-207.
 6. Miano JM. Serum response factor: Toggling between disparate programs of gene expression. *J Mol Cell Cardiol*. 2003;35:577-593.
 7. Wang DZ, Li S, Hockemeyer D, Sutherland L, Wang Z, Schratt G, Richardson JA, Nordheim A, Olson EN. Potentiation of serum response factor activity by a family of myocardin-related transcription factors. *Proc Natl Acad Sci U S A*. 2002;99:14855-14860.
 8. Guettler S, Vartiainen MK, Miralles F, Larijani B, Treisman R. Rpel motifs link the serum response factor cofactor mal but not myocardin to rho signaling via actin binding. *Mol Cell Biol*. 2008;28:732-742.
 9. Miralles F, Posern G, Zaromytidou AI, Treisman R. Actin dynamics control srf activity by regulation of its coactivator mal. *Cell*. 2003;113:329-342.
 10. Miano JM, Ramanan N, Georger MA, de Mesy Bentley KL, Emerson RL, Balza RO, Jr., Xiao Q, Weiler H, Ginty DD, Misra RP. Restricted inactivation of serum response factor to the cardiovascular system. *Proc Natl Acad Sci U S A*. 2004;101:17132-17137.
 11. Mokalled MH, Carroll KJ, Cenik BK, Chen B, Liu N, Olson EN, Bassel-Duby R. Myocardin-related transcription factors are required for cardiac development and function. *Dev Biol*. 2015;406:109-116.
 12. Oh J, Richardson JA, Olson EN. Requirement of myocardin-related transcription factor-b for remodeling of branchial arch arteries and smooth muscle differentiation. *Proc Natl Acad Sci U S A*. 2005;102:15122-15127.
 13. Small EM, O'Rourke JR, Moresi V, Sutherland LB, McAnally J, Gerard RD, Richardson JA, Olson EN. Regulation of pi3-kinase/akt signaling by muscle-enriched microRNA-486. *Proc Natl Acad Sci U S A*. 2010;107:4218-4223.
 14. Zhao X, Ding EY, Yu OM, Xiang SY, Tan-Sah VP, Yung BS, Hedgpeth J, Neubig RR, Lau LF, Brown JH, Miyamoto S. Induction of the matricellular protein ccn1 through rhoa and mrtf-a contributes to ischemic cardioprotection. *J Mol Cell Cardiol*. 2014;75:152-161.
 15. Kuwahara K, Kinoshita H, Kuwabara Y, Nakagawa Y, Usami S, Minami T, Yamada Y, Fujiwara M, Nakao K. Myocardin-related transcription factor a is a common mediator of mechanical stress- and neurohumoral stimulation-induced cardiac hypertrophic signaling leading to activation of brain natriuretic peptide gene expression. *Mol Cell Biol*. 2010;30:4134-4148.
 16. Olson EN, Nordheim A. Linking actin dynamics and gene transcription to drive cellular motile functions. *Nat Rev Mol Cell Biol*. 2010;11:353-365.
 17. Lyon RC, Zanella F, Omens JH, Sheikh F. Mechanotransduction in cardiac hypertrophy and failure. *Circ Res*. 2015;116:1462-1476.
 18. Li J, Patel VV, Kostetskii I, Xiong Y, Chu AF, Jacobson JT, Yu C, Morley GE, Molkentin JD, Radice GL. Cardiac-specific loss of n-cadherin leads to alteration in connexins with conduction slowing and arrhythmogenesis. *Circ Res*. 2005;97:474-481.

19. Oxford EM, Musa H, Maass K, Coombs W, Taffet SM, Delmar M. Connexin43 remodeling caused by inhibition of plakophilin-2 expression in cardiac cells. *Circ Res.* 2007;101:703-711.
20. Chen SN, Gurha P, Lombardi R, Ruggiero A, Willerson JT, Marian AJ. The hippo pathway is activated and is a causal mechanism for adipogenesis in arrhythmogenic cardiomyopathy. *Circ Res.* 2014;114:454-468.
21. Garcia-Gras E, Lombardi R, Giocondo MJ, Willerson JT, Schneider MD, Khoury DS, Marian AJ. Suppression of canonical wnt/beta-catenin signaling by nuclear plakoglobin recapitulates phenotype of arrhythmogenic right ventricular cardiomyopathy. *J Clin Invest.* 2006;116:2012-2021.
22. Seeger TS, Frank D, Rohr C, Will R, Just S, Grund C, Lyon R, Luedde M, Koegl M, Sheikh F, Rottbauer W, Franke WW, Katus HA, Olson EN, Frey N. Myozap, a novel intercalated disc protein, activates serum response factor-dependent signaling and is required to maintain cardiac function in vivo. *Circ Res.* 2010;106:880-890.
23. Asimaki A, Kapoor S, Plovie E, Karin Arndt A, Adams E, Liu Z, James CA, Judge DP, Calkins H, Churko J, Wu JC, MacRae CA, Kleber AG, Saffitz JE. Identification of a new modulator of the intercalated disc in a zebrafish model of arrhythmogenic cardiomyopathy. *Sci Transl Med.* 2014;6:240ra274.
24. Rangrez AY, Eden M, Poyanmehr R, Kuhn C, Stiebeling K, Dierck F, Bernt A, Lullmann-Rauch R, Weiler H, Kirchof P, Frank D, Frey N. Myozap deficiency promotes adverse cardiac remodeling via differential regulation of mitogen-activated protein kinase/serum-response factor and beta-catenin/gsk-3beta protein signaling. *J Biol Chem.* 2016;291:4128-4143.
25. Wang Q, Lin JL, Chan SY, Lin JJ. The xin repeat-containing protein, mxinbeta, initiates the maturation of the intercalated discs during postnatal heart development. *Dev Biol.* 2013;374:264-280.
26. Sohal DS, Nghiem M, Crackower MA, Witt SA, Kimball TR, Tymitz KM, Penninger JM, Molkenstein JD. Temporally regulated and tissue-specific gene manipulations in the adult and embryonic heart using a tamoxifen-inducible cre protein. *Circ Res.* 2001;89:20-25.
27. Mokalled MH, Johnson A, Kim Y, Oh J, Olson EN. Myocardin-related transcription factors regulate the cdk5/pctaire1 kinase cascade to control neurite outgrowth, neuronal migration and brain development. *Development.* 2010;137:2365-2374.
28. Li S, Chang S, Qi X, Richardson JA, Olson EN. Requirement of a myocardin-related transcription factor for development of mammary myoepithelial cells. *Mol Cell Biol.* 2006;26:5797-5808.
29. Zhao XH, Laschinger C, Arora P, Szaszi K, Kapus A, McCulloch CA. Force activates smooth muscle alpha-actin promoter activity through the rho signaling pathway. *J Cell Sci.* 2007;120:1801-1809.
30. Zhou Y, Huang X, Hecker L, Kurundkar D, Kurundkar A, Liu H, Jin TH, Desai L, Bernard K, Thannickal VJ. Inhibition of mechanosensitive signaling in myofibroblasts ameliorates experimental pulmonary fibrosis. *J Clin Invest.* 2013;123:1096-1108.
31. Balza RO, Jr., Misra RP. Role of the serum response factor in regulating contractile apparatus gene expression and sarcomeric integrity in cardiomyocytes. *J Biol Chem.* 2006;281:6498-6510.

32. Kanisicak O, Khalil H, Ivey MJ, Karch J, Maliken BD, Correll RN, Brody MJ, SC JL, Aronow BJ, Tallquist MD, Molkentin JD. Genetic lineage tracing defines myofibroblast origin and function in the injured heart. *Nat Commun.* 2016;7:12260.
33. Kostin S, Rieger M, Dammer S, Hein S, Richter M, Klovekorn WP, Bauer EP, Schaper J. Gap junction remodeling and altered connexin43 expression in the failing human heart. *Mol Cell Biochem.* 2003;242:135-144.
34. Leo-Macias A, Agullo-Pascual E, Sanchez-Alonso JL, Keegan S, Lin X, Arcos T, Feng Xia L, Korchev YE, Gorelik J, Fenyo D, Rothenberg E, Rothenberg E, Delmar M. Nanoscale visualization of functional adhesion/excitability nodes at the intercalated disc. *Nat Commun.* 2016;7:10342.
35. Shaw RM, Fay AJ, Puthenveedu MA, von Zastrow M, Jan YN, Jan LY. Microtubule plus-end-tracking proteins target gap junctions directly from the cell interior to adherens junctions. *Cell.* 2007;128:547-560.
36. Chkourko HS, Guerrero-Serna G, Lin X, Darwish N, Pohlmann JR, Cook KE, Martens JR, Rothenberg E, Musa H, Delmar M. Remodeling of mechanical junctions and of microtubule-associated proteins accompany cardiac connexin43 lateralization. *Heart Rhythm.* 2012;9:1133-1140 e1136.
37. Basheer WA, Xiao S, Epifantseva I, Fu Y, Kleber AG, Hong T, Shaw RM. Gja1-20k arranges actin to guide cx43 delivery to cardiac intercalated discs. *Circ Res.* 2017;121:1069-1080.
38. Esnault C, Stewart A, Gualdrini F, East P, Horswell S, Matthews N, Treisman R. Rho-actin signaling to the mrtf coactivators dominates the immediate transcriptional response to serum in fibroblasts. *Genes Dev.* 2014;28:943-958.
39. Parlakian A, Charvet C, Escoubet B, Mericskay M, Molkentin JD, Gary-Bobo G, De Windt LJ, Ludosky MA, Paulin D, Daegelen D, Tuil D, Li Z. Temporally controlled onset of dilated cardiomyopathy through disruption of the srf gene in adult heart. *Circulation.* 2005;112:2930-2939.
40. Huang J, Min Lu M, Cheng L, Yuan LJ, Zhu X, Stout AL, Chen M, Li J, Parmacek MS. Myocardin is required for cardiomyocyte survival and maintenance of heart function. *Proc Natl Acad Sci U S A.* 2009;106:18734-18739.
41. Small EM, Warkman AS, Wang DZ, Sutherland LB, Olson EN, Krieg PA. Myocardin is sufficient and necessary for cardiac gene expression in xenopus. *Development.* 2005;132:987-997.
42. Agullo-Pascual E, Lin X, Leo-Macias A, Zhang M, Liang FX, Li Z, Pfenniger A, Lubkemeier I, Keegan S, Fenyo D, Willecke K, Rothenberg E, Delmar M. Super-resolution imaging reveals that loss of the c-terminus of connexin43 limits microtubule plus-end capture and nav1.5 localization at the intercalated disc. *Cardiovasc Res.* 2014;104:371-381.
43. Davis J, Davis LC, Correll RN, Makarewich CA, Schwanekamp JA, Moussavi-Harami F, Wang D, York AJ, Wu H, Houser SR, Seidman CE, Seidman JG, Regnier M, Metzger JM, Wu JC, Molkentin JD. A tension-based model distinguishes hypertrophic versus dilated cardiomyopathy. *Cell.* 2016;165:1147-1159.
44. Busche S, Descot A, Julien S, Genth H, Posern G. Epithelial cell-cell contacts regulate srf-mediated transcription via rac-actin-mal signalling. *J Cell Sci.* 2008;121:1025-1035.
45. Lauriol J, Keith K, Jaffre F, Couvillon A, Saci A, Goonasekera SA, McCarthy JR, Kessinger CW, Wang J, Ke Q, Kang PM, Molkentin JD, Carpenter C, Kontaridis MI.

- Rhoa signaling in cardiomyocytes protects against stress-induced heart failure but facilitates cardiac fibrosis. *Sci Signal*. 2014;7:ra100.
46. Corrado D, Link MS, Calkins H. Arrhythmogenic right ventricular cardiomyopathy. *N Engl J Med*. 2017;376:1489-1490.
 47. Kuwahara K, Teg Pipes GC, McAnally J, Richardson JA, Hill JA, Bassel-Duby R, Olson EN. Modulation of adverse cardiac remodeling by stars, a mediator of mef2 signaling and srf activity. *J Clin Invest*. 2007;117:1324-1334.
 48. Gaertner A, Schwientek P, Ellinghaus P, Summer H, Golz S, Kassner A, Schulz U, Gummert J, Milting H. Myocardial transcriptome analysis of human arrhythmogenic right ventricular cardiomyopathy. *Physiol Genomics*. 2012;44:99-109.
 49. Agullo-Pascual E, Reid DA, Keegan S, Sidhu M, Fenyö D, Rothenberg E, Delmar M. Super-resolution fluorescence microscopy of the cardiac connexome reveals plakophilin-2 inside the connexin43 plaque. *Cardiovasc Res*. 2013;100:231-240.



Circulation

Figure Legends

Figure 1. MRTF-A and –B are enriched at IDs and associate with desmosome proteins.

Immunohistochemistry for MRTF-A and –B (green) protein distribution during postnatal (P) development from 1 week (P7) to 8 weeks (P56). At three weeks (P21), MRTF localization is coincident with the maturation of intercalated discs, revealed by co-localization with plakophilin-2 (PKP2, red). MRTFs become highly restricted to the IDs by P56. ID staining is marked by white arrowheads. LV = left ventricle; epi = epicardium. Scale bar = 25µm.

Figure 2. Altered MRTF localization in human heart failure. **A**, Representative

immunohistochemistry for MRTFs (green) and plakophilin 2 (PKP2, red) in sections from the left ventricle of a healthy (control) or failing (heart failure) human heart. MRTFs are more diffusely distributed in the diseased myocardium with occasional nuclear accumulation denoted by white arrowheads. Trichrome staining reveals fibrotic remodeling (blue) with heart failure. Scale bar = 30 µm. **B**, Representative orthogonal view of a confocal Z-stack projection

demonstrating MRTF localization in a Dapi-positive CM nucleus (white arrowhead). Scale bar =

10 µm. **C - D**, Co-immunoprecipitation (Co-IP) studies were conducted using COS-7 cells

transfected with epitope tagged PKP2-FLAG and MRTF-A-HA. (C) MRTF-A

immunoprecipitates PKP2 and endogenous actin. Actin immunoprecipitation is reduced upon

PKP2 overexpression. (D) Immunoprecipitation of MRTF-A by endogenous actin is reduced

upon overexpression of PKP2. The Co-IP data is representative of two to three independent

experiments.

Figure 3. MRTF^{dKO} mice deteriorate in response to pressure overload induced by TAC. A, Experimental timeline for cardiac-specific depletion of MRTFs and heart failure studies. Serial echocardiography was conducted for 28 days post-surgery. **B,** Kaplan-Meier survival analysis of MRTF^{dKO} and control mice after TAC surgery. $P < 0.01$, Log-Rank (Mantel-Cox) test. $n = 4$ (control sham), 3 (MRTF^{dKO} sham), 9 (control TAC), and 15 (MRTF^{dKO} TAC). **C – D,** Longitudinal echocardiographic analysis of percent fractional shortening (FS, C) and ejection fraction (EF, D). $n = 6$ (control sham), 12 (control TAC), 3 (MRTF^{dKO} sham), and 3 (MRTF^{dKO} TAC). **E,** Heart weight to tibia length ratios (HW:TL) measured 28 days after TAC surgery. $n = 6$ (control sham), 12 (control TAC), 4 (MRTF^{dKO} sham), and 7 (MRTF^{dKO} TAC). **F,** Representative hematoxylin and eosin staining of control or MRTF^{dKO} hearts 28 days after TAC or sham surgery. Scale bars = 1mm. **G – J,** qRT-PCR analysis of heart failure genes (*Myh6*, *Myh7*, *Nppb* and *Acta1*) in hearts from control or MRTF^{dKO} mice 28 days after TAC. All quantified data represents the mean \pm SEM. All statistics were performed with two-way ANOVA and Tukey post-hoc tests. Echo data was analyzed with two-way repeated measures ANOVA. Asterisks denote significance with $*P < 0.05$, $**P < 0.01$, $***P < 0.001$, or $****P < 0.0001$. Statistical significance of a given genotype compared to day 0 is denoted by $\dagger P < 0.01$, $\ddagger P < 0.001$, and $\# P < 0.0001$.

Figure 4. MRTF^{dKO} hearts undergo dilation in response to pressure overload. A – H, Left ventricular (LV) end systolic (s) and diastolic (s) volumes (LVESV, A; LVEDV, B), internal diameters (LVIDs, C; LVIDd, D), anterior wall diameters (LVAWDs, E; LVAWDd, F), and posterior wall diameters (LVPWDs, G; LVPWDd, H). The data represents the mean \pm SEM. $n = 6$ (control sham), 12 (control TAC), 3 (MRTF^{dKO} sham), and 3 (MRTF^{dKO} TAC). **I,** CM

morphology was assessed by wheat germ agglutinin (WGA, red) staining to label the lateral edges and Cx43 (green) to label IDs. Nuclei are labeled by DAPI (blue). Scale bar = 30 μm . **J–L**, Violin plots represent quantification of CM dimensions in (I) by length (J), width (K) and length-to-width (L) ratios. $n = 3$ hearts per group with 300-400 CM measured per heart. All statistics were performed with two-way ANOVA and Tukey post-hoc tests. Echo data was analyzed with two-way repeated measures ANOVA. Asterisks denote significance with $*P < 0.05$, $**P < 0.01$, $***P < 0.001$, or $****P < 0.0001$. Statistical significance of a given genotype compared to day 0 is denoted by $\S P < 0.05$, $\dagger P < 0.01$, $\ddagger P < 0.001$, and $\# P < 0.0001$.

Figure 5. MRTF deletion disrupts ID integrity and sarcomere organization. A - A'

Electron micrographs of MRTF^{dKO} and control hearts 28 days after TAC or sham surgery. White boxes in (A) represent regions magnified in (A'). IDs appear more convoluted in MRTF^{dKO} sham hearts compared to controls (a, a' – b, b'). TAC injury further accentuates distortion to MRTF^{dKO} IDs as evident by increased plicae and unorganized connections between the myofibrils and ID (c, c' – d, d'). Scale bars = 1 μm (A) or 0.5 μm (A'). **B**, Ultrastructural analysis reveals conspicuous alterations in sarcomere arrangement with MRTF deletion and cardiac stress. In comparison to control TAC hearts, MRTF^{dKO} hearts have more diffuse Z-discs (black arrowhead), barely detectable M-lines (white arrowhead), and unclear demarcations between the A-bands (white bracket) and I bands (black bracket). In addition, the distance between adjacent Z-discs is shorter in MRTF^{dKO} TAC hearts compared to controls. Scale bars = 0.5 μm . **C**, Violin plots represent quantification of sarcomere length measured between adjacent Z-discs within TEM micrographs of control and MRTF^{dKO} hearts, 28 days after TAC. Each point represents an individual sarcomere with the group mean denoted by the black bar. $n = 3$ hearts per group with

200 - 400 sarcomeres measured per group. Statistics were performed with two-way ANOVA and Tukey post-hoc tests. Asterisks denote significance with **** $P < 0.0001$.

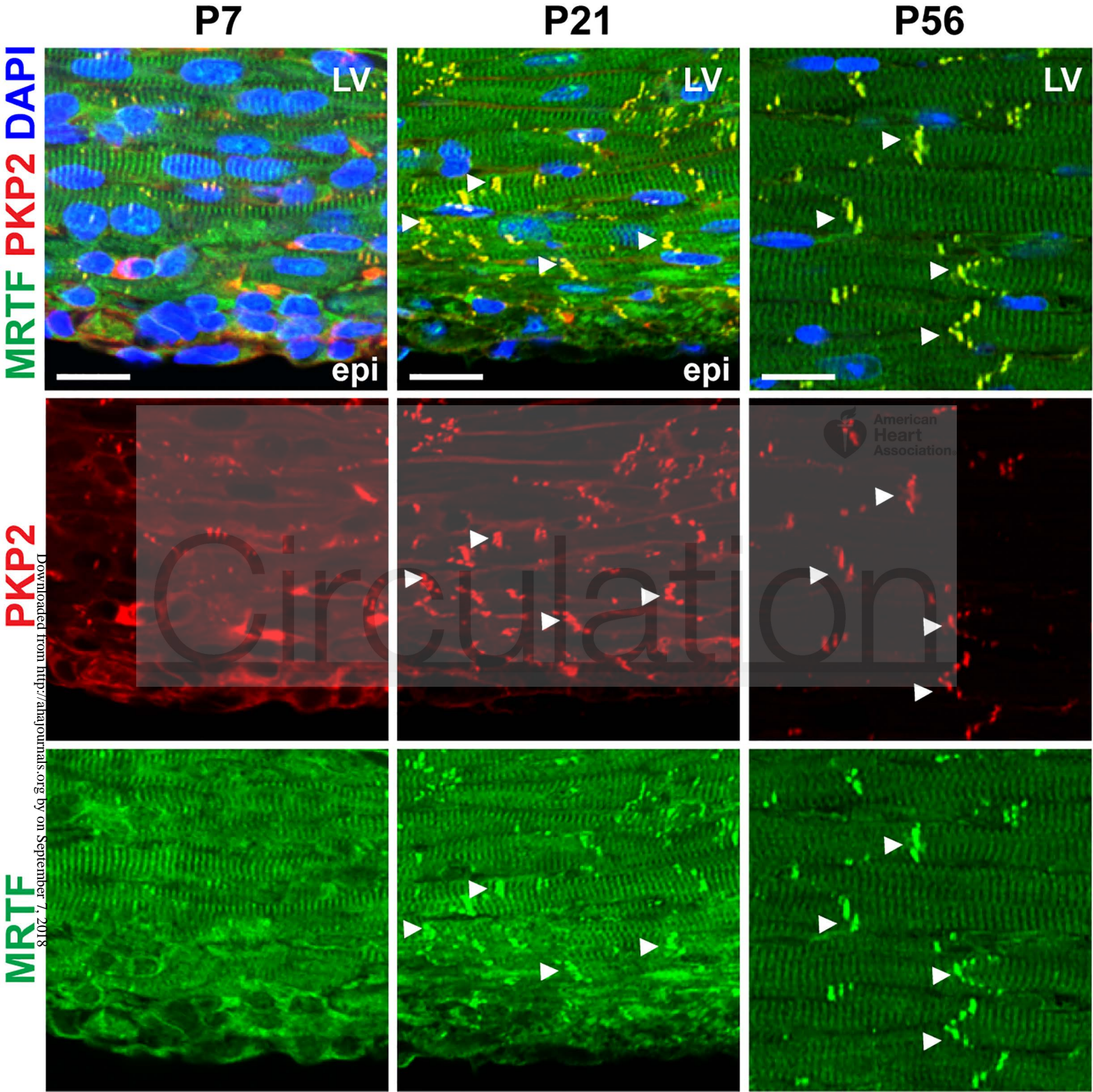
Figure 6. MRTF ablation perturbs gap junction trafficking to IDs. **A**, Representative SMLM image of Cx43 (purple) and N-cadherin (green) in CMs isolated from 10 week old mice 2 weeks after tamoxifen administration. The highlighted area along ID plicate denotes the region of interest (ROI) for SMLM quantification. Scale bar = 5 μ m. **B**, Quantification of the number of Cx43 clusters per ROI from control or MRTF^{dKO} CMs. Cx43 clusters are less dense at the ID with MRTF depletion. Only Cx43 clusters within a distance of 500nm to the nearest neighbor were included for analysis. **C**, The proximity of a given Cx43 cluster to the nearest Cx43 cluster is significantly reduced with MRTF deletion (B – C). $n = 7$ (control), 9 (MRTF^{dKO}). Statistics were performed using a student t-test. * $P < 0.05$, *** $P < 0.001$. **D**, Representative SMLM image of EB1 (purple) and N-cadherin (green) in CMs isolated from 10 week old mice 2 weeks after tamoxifen administration. **D'** Magnified view of (D) shows EB1 measurements with respect to ID. Dashed line represents ID surface defined by N-cadherin staining. Yellow line indicates EB1 distance measured. Arrows indicate cluster classification: (1 and 4) ID = overlapping reference line or N-cadherin cluster, (2) distal = less than 500 nm from reference line, (3) discarded = not adjacent to or greater than 500nm from reference line. **E**, Histogram of EB1 proximity to the ID. EB1 is located more distal with respect to the ID in CMs isolated from MRTF^{dKO} hearts compared to controls.

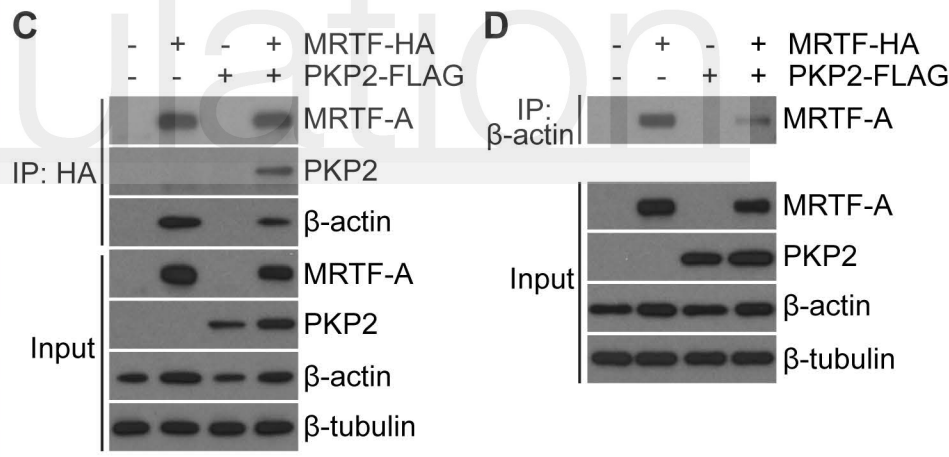
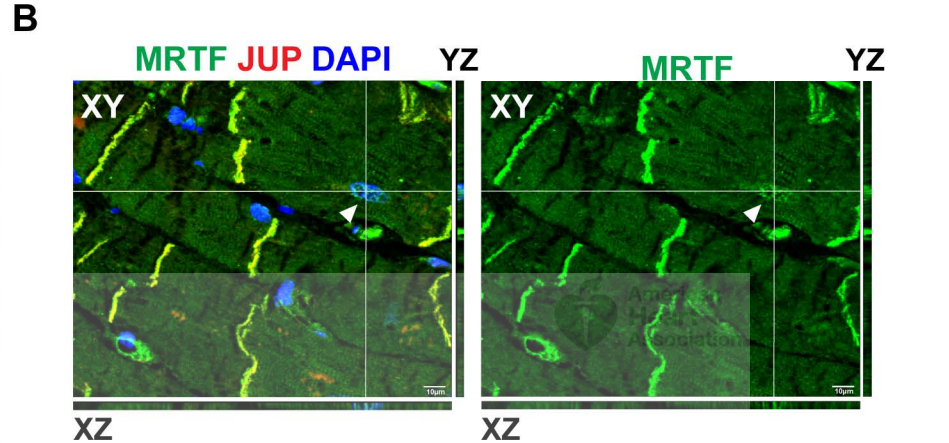
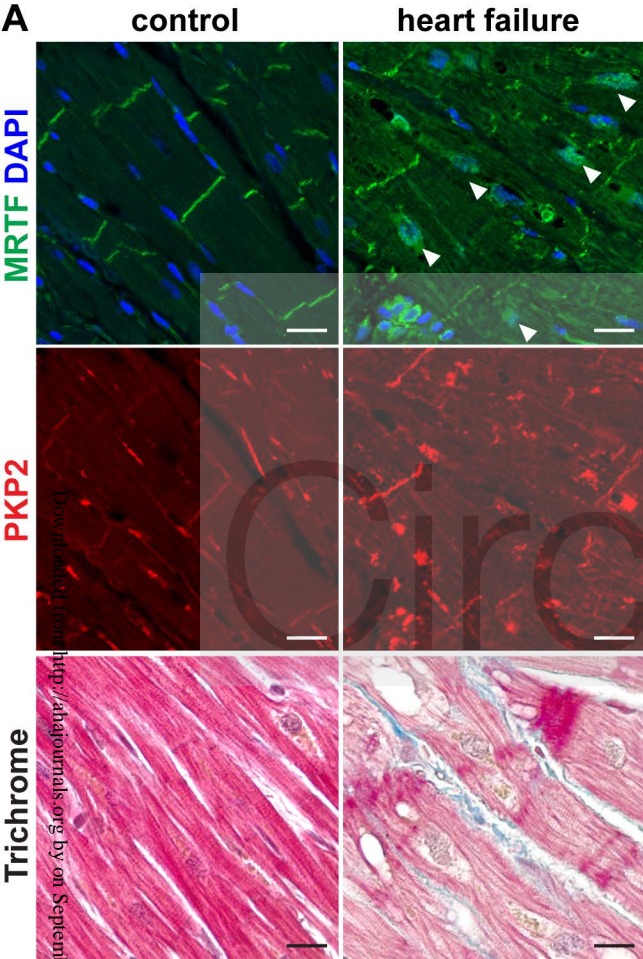
Figure 7. RNA-seq analysis reveals dysregulated cytoskeletal and adhesion pathways in MRTF^{dKO} TAC myocytes. **A**, MRTF^{dKO} and control CM were isolated 7 days after TAC or

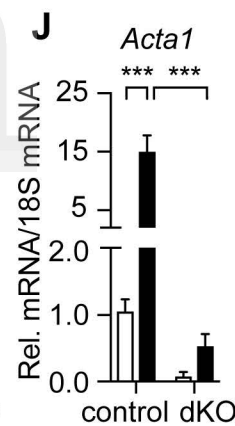
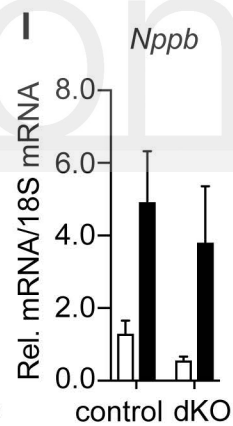
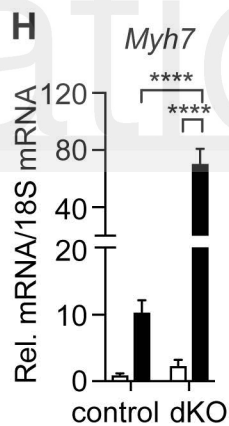
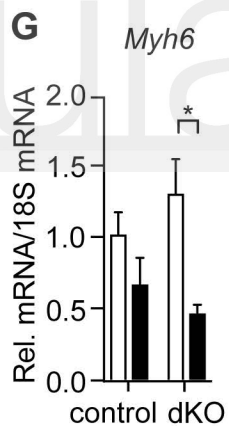
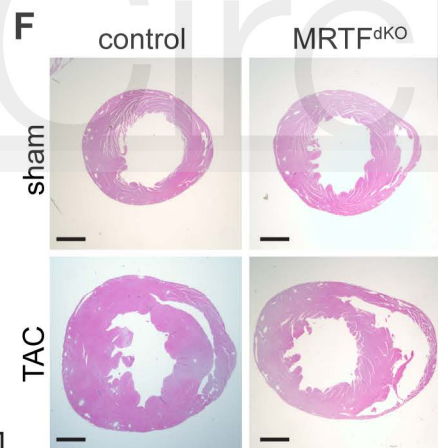
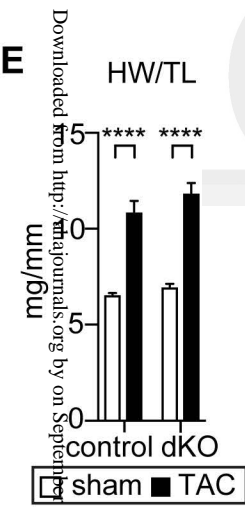
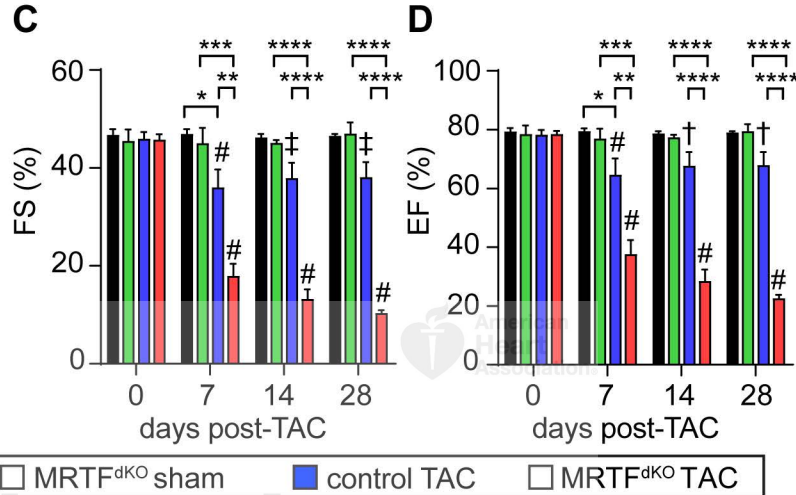
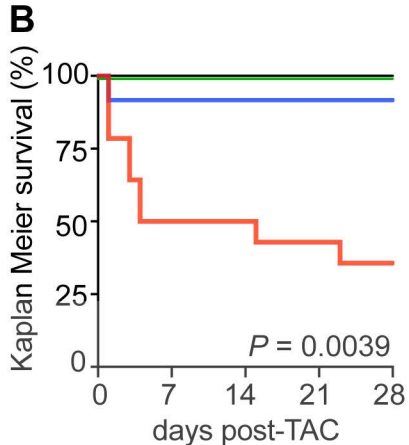
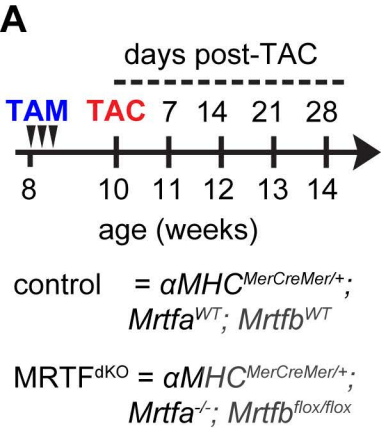
sham surgery for RNA-seq analysis as shown in the experimental timeline. A comparison of differentially expressed genes (DEG, $q < 0.05$) for each comparison as depicted by black arrows between groups. Up-regulated genes are labeled in red and down-regulated genes are shown in blue. **B – C**, Ingenuity Pathway Analysis (IPA) of DEGs between MRTF^{dKO} and control TAC myocytes (red box in (A)). The data represents the top 15 upstream transcription factors (B) and signaling pathways (C) predicted to be altered with MRTF deletion. Ontology terms are organized by significance as $-\log_{10}(P\text{-value})$. The color bar represents the predicted activation Z-score of a given pathway or transcription factor, where red denotes activated and blue represents inhibited. **D – E**, Gene ontology analysis of the top 4 biological processes (D) and cellular compartment terms (E) altered in MRTF^{dKO} TAC myocytes reveals dysregulation of muscle contraction and structural components of the ID and adherens junctions. Ontology terms are organized according to significance as $-\log_{10}(q\text{-value})$. The red lines (D, E) represent where $P = 0.05$. **F**, Hierarchical clustering of 347 DEGs between MRTF^{dKO} and control TAC myocytes. Each row represents the average gene expression between three biological replicates per group and each column represents an individual gene. The color bar indicates relative expression levels of log-transformed, normalized counts with up-regulated genes shown in red and down-regulated genes shown in blue. A cluster of genes up-regulated in control TAC myocytes and significantly down-regulated with MRTF deletion is expanded below. **G – J**, Control and MRTF^{dKO} NVMs were subjected to 20% unilateral stretch for 4 hours. prior to evaluating the expression of candidate MRTF target genes by qRT-PCR. The data represents three technical replicates from NVMs derived from two pooled litters per genotype. Statistics were performed with a two-way ANOVA and Tukey post-hoc tests. Asterisks denote significance with $**P < 0.01$, $***P < 0.001$, or $****P < 0.0001$.

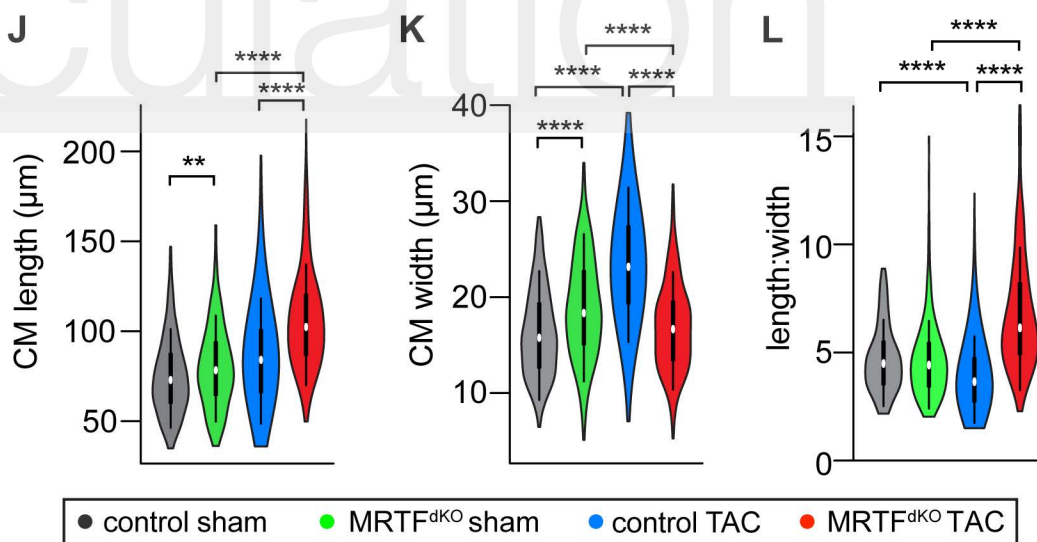
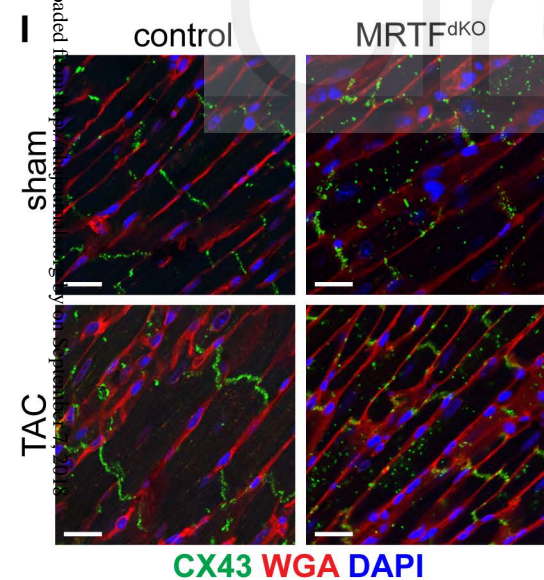
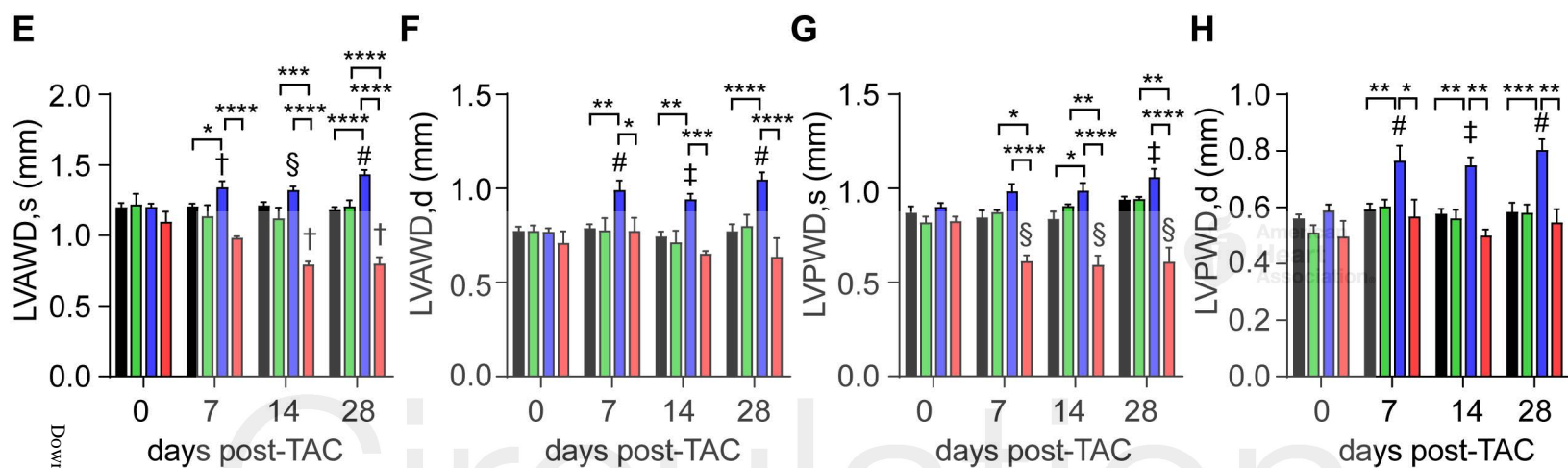
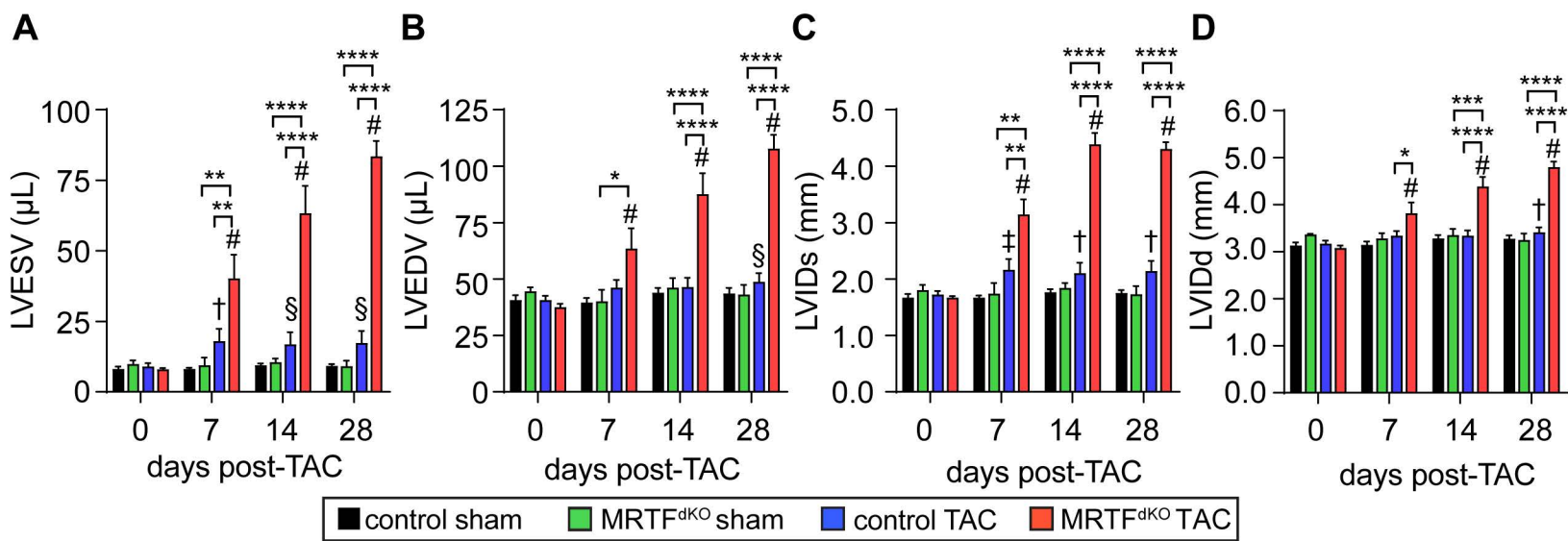
Figure 8. Stretch-dependent activation of *Mapre1* requires MRTF/SRF dependent

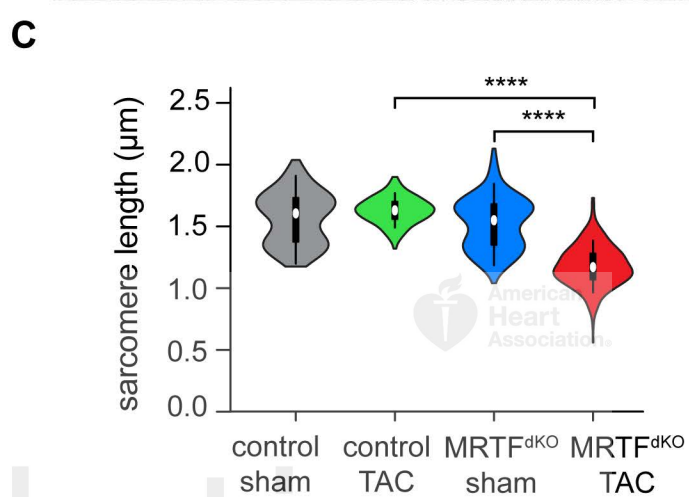
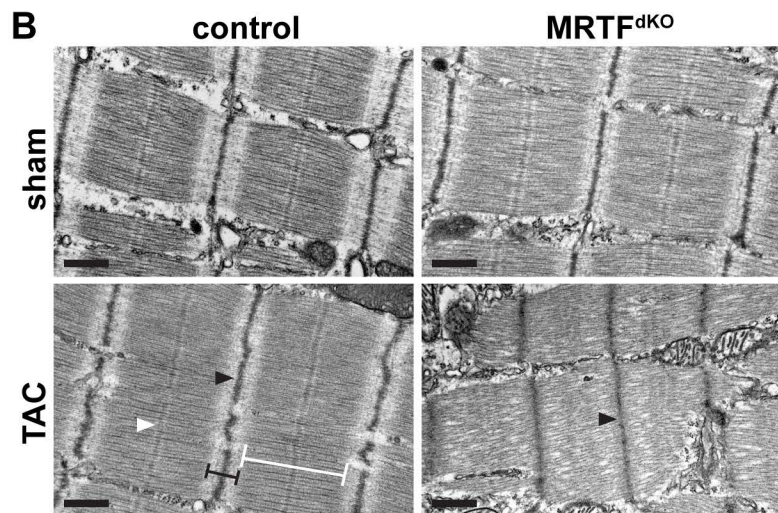
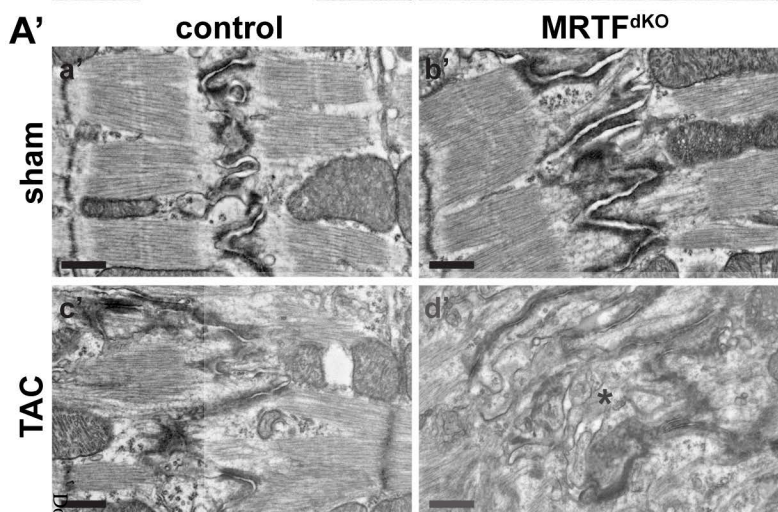
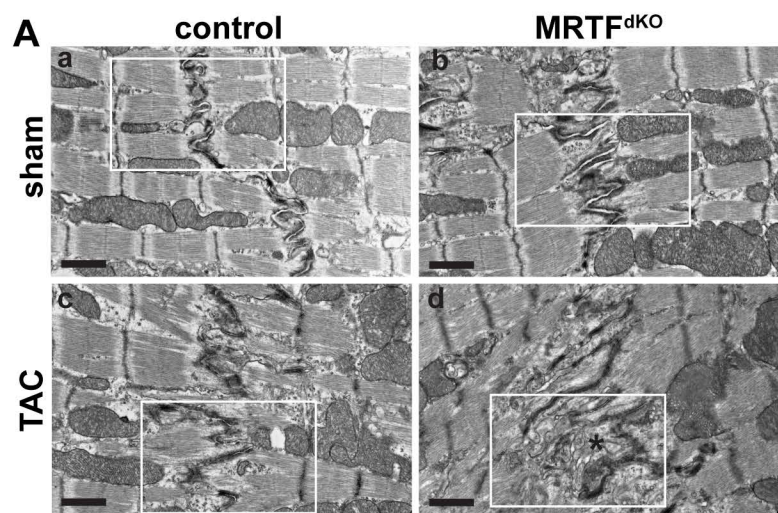
transcription. A, qRT-PCR of Cx43 (*Gjal*) and gap junction trafficking genes (*Mapre1*, *Kif5b*, *Dctn1*) from adult CMs isolated from MRTF^{dKO} and control hearts 14 days post-tamoxifen injection. n = 3 controls and 4 MRTF^{dKO}. **B**, qRT-PCR of C57BL/6 NVMs transduced with a control adenovirus or an adenovirus expressing MRTF-A and cultured for 48 hours. n = 9 (*Acta2*, *Mapre1*, *Dctn1*), 3 (*Kif5b*). **C**, MRTFs are required for stretch-induced expression of *Mapre1* in NVMs subject to 20% uniaxial stretch for 4 hrs. The data represents three technical replicates from NVMs derived from two pooled litters per genotype. **D**, Analysis of the mouse *Mapre1* gene using the UCSC genome browser reveals an evolutionarily conserved CArG motif -33 to -24 nucleotides upstream of the transcription start site (+1). Exons (E) are labeled in green. Conserved regions are shown in blue. Sequence of conserved CArG box and mutation is noted below. **E**, MRTF-mediated induction of *Mapre1*-luciferase requires the CArG motif. The data represents the combination of three independent experiments. **F**, ChIP reveals SRF occupancy at the *Mapre1* promoter. ChIP for *Acta2* is included as a positive control for SRF occupancy. ChIP experiments were performed from C56BL/6 whole heart lysates. The data represents the combination of three independent experiments. All data represents the mean ± SEM. Statistics in (A, B, F) were performed using a student t-test. Statistics in (C, E) using a two-way ANOVA and Tukey post-hoc tests. *P < 0.05, **P < 0.01, ***P < 0.001, ****P < 0.0001.



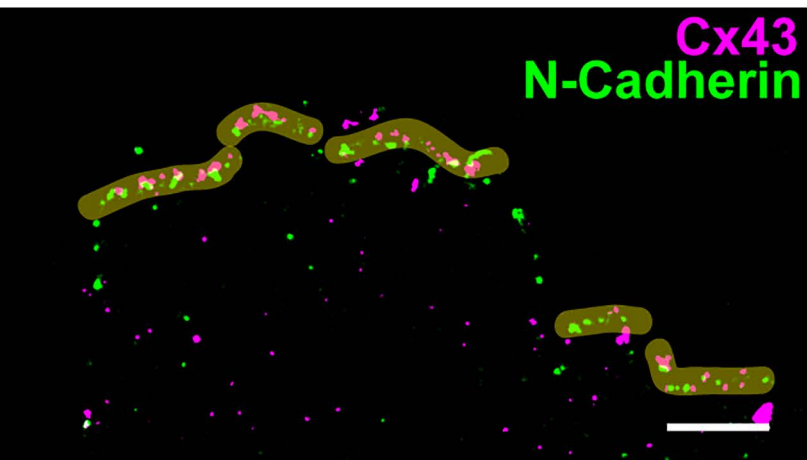
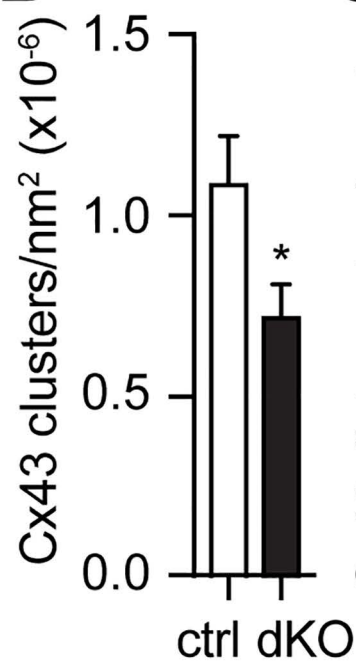
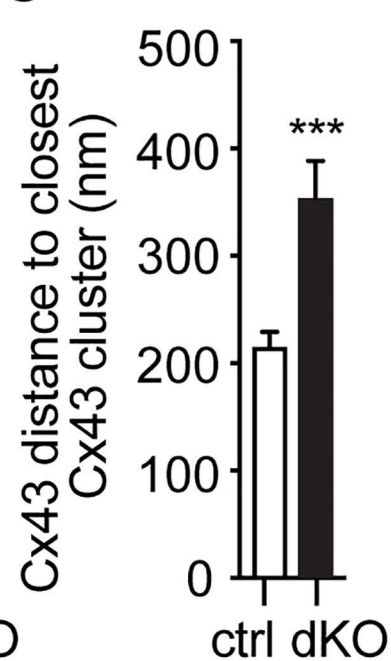
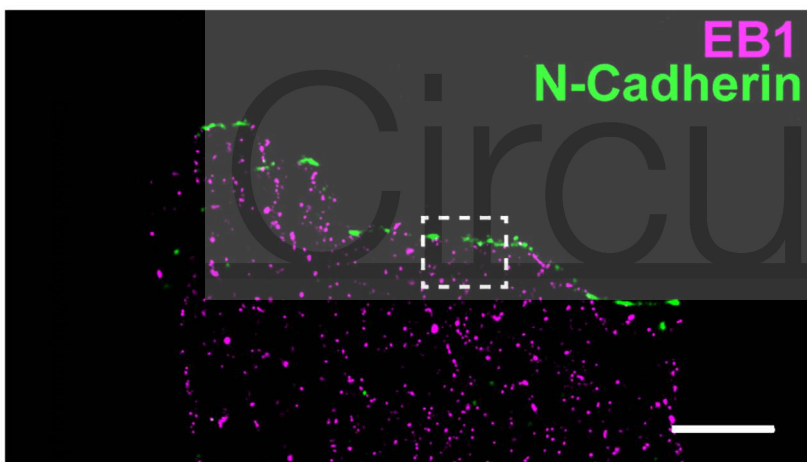
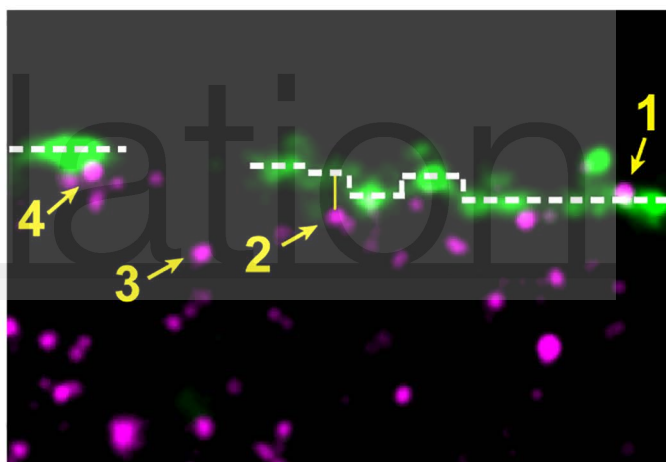








Circulation

A**B****C****D****D'****E**